PERGAMON International Journal of Engineering Science 39 (2001) 1597–1615

International Journal of Engineering Science

www.elsevier.com/locate/ijengsci

A mesoscopic model for inelastic deformation and damage

Ismail Demir [a], Hussein M. Zbib [b,*]

[a] *Department of Mechanical Engineering, King Saud University, Riyadh 11421, Saudi Arabia*
[b] *School of Mechanical and Materials Engineering, Washington State University, Pullman, WA 99164-2920, USA*

Received 18 August 1999; accepted 18 October 2000

Abstract

The micro-mechanical behavior and damage of materials containing multiple microcracks is investigated using a mesoscopic approach. We develop an analytical and computational framework for the nucleation and interaction of microcracks near a macrocrack tip based on both the theory of elasticity and the theory of dislocations. Grain boundaries are considered as critical material points for crack initiation. The discrete model is used to investigate the relationship between the macroscopic applied stress and evolution of microcracks, yielding a micro-structurally based model for the evolution of damage consistent with some theoretical models. It is suggested that with this approach macroscopic models can be developed whose phenomenological parameters can be rigorously investigated and obtained using discrete simulation of microcracks.

1. Introduction

Many lightweight materials such as ceramics have the potential for a wide range of engineering applications that would result in tremendous cost and energy benefits. However, one of the main limitations is the susceptibility of these materials to microcracking, limiting ductility and causing failure. Therefore, many researchers [1–7] have spent a great deal of effort in investigating problems involving the mechanical behavior of materials containing multiple cracks. However, in the majority of these solutions extreme simplifications have been introduced and some facts have been overlooked. For instance the exact formulation of the crack–defect interaction problem, shielding at the crack tips and amplification of the stress intensity factors and interaction with other defects have not been accurately analyzed. Studies such as those given in [1] attempted to model nucleation of cracks. However, they failed to model the exact interaction process. Some

* Corresponding author. Tel.: +1-509-335-7832; fax: +1-509-335-4662.
E-mail address: zbib@mme.wsu.edu (H.M. Zbib).

0020-7225/01/$ - see front matter
PII: S0020-7225(01)00003-9

other studies managed to model the interaction problem more accurately [3–5] but included a number of simplifications that limited the applicability of the models. This issue has recently been revisited in [8] and a more rigorous treatment of the interaction problem between two cracks has been presented.

In the present work we address the problem of multiple planar cracks in an infinite domain under mixed mode loading conditions. It may be apparent that the mutual interaction among multiple cracks could significantly alter the stress field and, therefore, would affect related stress intensity factors at the crack tips. Therefore, results pertaining to a single crack cannot be simply used when dealing with multiple microcracks, especially, when the microcrack density is relatively large, leading to strong interactions. Although, the problem addressed in this paper is for the planar case, it can be extended straightforwardly to other types of cracks in three-dimensional cases [9,10]. Furthermore, the formulation of the interaction of not only multiple cracks but also other defects such as dislocations, inclusions and voids could follow. In the case of cracks in ductile materials, dislocation motion around the multiple cracks can be formulated on the same basis. This is an interesting topic that could provide a more rigorous approach to the problem of plastic zone around the crack tips as presented in [11].

The specific application of crack nucleation and propagation problem in polycrystalline is considered. With increasing loads nucleation of microcracks could be considered as a toughening mechanisms in brittle materials. If a macrocrack pre-exist in a polycrystalline material it is expected that this crack would grow and/or some new microcracks would nucleate around the tips of the main crack. The stress field would control that process. Crack generation or propagation is determined by employing a certain criteria. For example, grain boundaries provide weak sites for the nucleation of new cracks. Moreover wedge cracks at triple junctions are frequently observed in these types of materials. In ductile materials pile up of dislocations at grain boundaries or triple junction disclinations could also serve as crack nucleation sites.

Following the idea presented in [1], certain material points are specified around a main crack tip. Each point is assigned a random orientation corresponding to a grain boundary representing a prospective crack initiation site and orientation. Then the stress field is analyzed throughout the domain and whenever the local stress reaches a critical (normal or shear) value a microcrack is initiated with a length corresponding to a representative size of a grain boundary. At each load level the analysis is repeated until no more new microcracks can be nucleated. Then the load is increased one more step and the process is continued until all possible sites are cracked or the stress intensity factor (SIF) value at the main crack tip exceeds a critical value. The entire model is based on continuum mechanics and linear theory of elasticity of a homogeneous medium. Cracks are represented by distributions of dislocations. This microscopic modeling yields a non-linear load deflection behavior in a non-homogeneous medium. This formulation results in a set of coupled integral equations that are solved numerically.

The primary goal of this line of work is to model different types of interacting defects together with dislocation dynamics around these defects in 2D and 3D cases [12]. This is expected to generate accurate estimation of the responses of the material such as load–deflection relations, damage history and stress field and failure mechanism so that, damage generation and propagation and its results on the global response can be better understood.

2. Formulation of the mesoscopic damage model

2.1. Stress field due to a single dislocation and a single crack

We employ the theory of dislocation pile-ups to model the stress field induced by a loaded crack. Consider a pair of glide and climb edge dislocations. The stresses due to these two dislocations are given in polar coordinates as [13]:

$$\begin{aligned}
\sigma_{rr} &= -Db_1\frac{\cos\theta}{r} + Db_2\frac{\sin\theta}{r},\\
\sigma_{\theta\theta} &= -Db_1\frac{\cos\theta}{r} + Db_2\frac{\sin\theta}{r},\\
\sigma_{r\theta} &= -Db_1\frac{\sin\theta}{r} + Db_2\frac{\sin\theta}{r},
\end{aligned} \tag{1}$$

where r and θ are polar coordinates, $b_1 (= u_{\theta_{\theta=0}} - u_{\theta_{\theta=2\pi}})$ and $b_2 (= u_{r_{\theta=0}} - u_{r_{\theta=2\pi}})$ are climb and glide components of the Burgers vector of a dislocation located at the origin, respectively, and u_θ, u_r are displacements components. The factor D which includes the shear modulus μ and Poisson's ratio v is expressed as $D = 2\mu/\pi(\kappa+1)$, where $\kappa = 3-4v$ for plane strain, and $\kappa = (3-v)/(1+v)$ for plane stress.

Following a standard approach and using the basic expressions for a single dislocation as Green's function, the stress field induced by continuous distributions of dislocation densities, that are used to represent a crack in an infinite medium, can be expressed as follows:

$$-D\int_{-a_1}^{a_1}\frac{b_1(s)}{(x-s)}\,\mathrm{d}s = -\sigma_0, \tag{2}$$

$$-D\int_{-a_1}^{a_1}\frac{b_2(s)}{(x-s)}\,\mathrm{d}s = -\tau_0 \tag{3}$$

where a_1 is the half length of the crack and x is a coordinate chosen along the crack line ($x \equiv r, \theta = 0$). The terms σ_0 and τ_0 are the normal and tangential components of the external distributed load acting at infinity and represent normal and tangential tractions along the crack faces applying the well-known superposition technique.

2.2. The crack interaction problem

In order to model the interaction of more than one crack, the above formulation given by (2) and (3) is repeated for each individual crack. We consider a medium with randomly oriented m microcracks. Then, due to the interactions among all microcracks, each one of them will feel the effect of all the others in addition to the externally applied stresses. Thus, σ_0 and τ_0 are replaced by the normal and tangential components of the external stresses and the effect of other microcracks

that include integral forms of the unknown dislocation densities. By repeating these equations for each one of the microcracks the following system of equations is obtained.

$$-D\int_{-a_{1i}}^{a_i}\frac{b_{n_i}(s_i)}{(x_i-s_i)}\,\mathrm{d}s_i=-\sigma_{0i}+D\sum_{j=1}^{m}\int_{-a_j}^{a_j}\left[b_{n_j}(s_j)N_{ij}^{n}(s_j,x_i)+b_{t_i}(s_j)T_{ij}^{n}(s_j,x_i)\right]\mathrm{d}s_j, \tag{4}$$

$$-D\int_{-a_i}^{a_i}\frac{b_{t_i}(s_i)}{(x_i-s_i)}\,\mathrm{d}s_i=-\tau_{0i}+D\sum_{j=1}^{m}\int_{-a_j}^{a_j}\left[b_{n_j}(s_j)N_{ij}^{t}(s_j,x_i)+b_{t_i}(s_j)T_{ij}^{t}(s_j,x_i)\right]\mathrm{d}s_j\quad i=1,\ldots,m, \tag{5}$$

where b_n and b_t are Burgers vectors of the corresponding dislocation density functions that are normal and parallel to the crack line. The right-hand sides of Eqs. (4) and (5) are for $i\neq j$. N and T are kernels containing the geometric parameters representing the position dependency of the influence of one crack on the other. Their exact forms are given in the Appendix A. The first terms on the right-hand sides of Eqs. (4) and (5), which show the effect of the external stresses, are defined as:

$$\sigma_{0i}=\sigma_0\cos\alpha_{c_i}^2+\tau_0\sin 2\alpha_{c_i}, \tag{6a}$$

$$\tau_{0i}=\frac{\sigma_0}{2}\sin 2\alpha_{c_i}+\tau_0\cos 2\alpha_{c_i}, \tag{6b}$$

where σ_0 and τ_0 are the normal and shear stress applied at infinity and α_{c_i} is the orientation angle of microcrack i. The repetition of the pair of integral equations m times gives $2m$ equations with $2m$ unknowns. In order to guarantee the uniqueness of the solution the following closure conditions must be imposed.

$$\int_{-a_i}^{a_i}b_{n_j}(s_i)\,\mathrm{d}s_i=0,\quad \int_{-a_i}^{a_i}b_{t_j}(s_i)\,\mathrm{d}s_i=0,\quad i=1,\ldots,m. \tag{7}$$

This completes the fully coupled exact formulation of the multiple crack interaction problem.

In the solution process, the above integrals are scaled using related microcrack half-length so that the limits are always between −1 and 1. Moreover, the space is scaled by the length of the macrocrack (when no macrocrack exists, scaling is with respect to grain size). In general these equations can be discretized and solved using one of many techniques available. The dislocation density distributions are separated into a singular and the regular parts as $b(s)=B(s)/\sqrt{1-s^2}$. In the present work the Chebyshev polynomial technique as proposed by Erdogan [14], among other techniques, is preferred due to its simplicity. When the crack propagation is added to the analysis, the quadratic polynomial technique could be preferred to relax the constraints on the scaling of the integral boundaries. The final forms of the discretized equations are given as:

$$\sum_{k=1}^{n}\left\{\frac{\bar{B}_{n_i}(s_{i,k})}{(x_{i,r}-s_{i,k})}+\left[\sum_{j=1}^{m}\bar{B}_{nj3}(s_{j,k})N_{ij}^{n}(s_{j,k},\hat{x}_{i,r})+\bar{B}_{t_j}(s_{j,k})T_{ij}^{n}(s_{j,k},\hat{x}_{i,r})\right]\right\}=\frac{\pi}{n}\bar{\sigma}_{0i}, \tag{8}$$

$$\sum_{k=1}^{n}\left\{\frac{\bar{B}_{t_i}(s_{i,k})}{(x_{i,r}-s_{i,k})}+\left[\sum_{j=1}^{m}\bar{B}_{n_j3}(s_{j,k})N_{ij}^{t}(s_{j,k},\hat{x}_{i,r})+\bar{B}_{t_j}(s_{j,k})T_{ij}^{t}(s_{j,k},\hat{x}_{i,r})\right]\right\}=\frac{\pi}{n}\bar{\tau}_{0i}, \tag{9}$$

where $\bar{B}_i=(D/\sigma_c)B_i$, $\bar{\tau}_{0i}=\tau_{0i}/\sigma_c$, $\bar{\sigma}_{0i}=\sigma_{0i}/\sigma_c$, and σ_c is some reference stress (here it is taken as the critical normal stress for crack nucleation). Moreover $s_{j,k}$ and $\hat{x}_{i,r}$'s are zeros of Chebyshev polynomials of the first and second kind, respectively. Indices i and j beside k and r indicate whether these points are along crack i or j. Because of non-dimensionalization in the local coordinates their values are the same at each equation. The number n is the number of nodal points along each crack. Additional equations are obtained from the discretized forms of the closure conditions.

$$\sum_{k=1}^{n}\bar{B}_{n_k}(s_{j,k})=0,\qquad \sum_{k=1}^{n}\bar{B}_{t_k}(s_{j,k})=0,\quad j=1,\ldots,m. \tag{10}$$

The edge or surface cracks are not covered in the above formulation. The formulation is restricted to the case of planar mixed mode cracks in an infinite domain where the external loads are uniformly distributed at infinity.

The present formulation gives result to the distribution of dislocation densities along the crack lines, which in turn can be used in calculating crack opening displacements, stress intensity factors and the entire extended stress field. It is important to note that once the distribution of dislocation density for each microcrack is obtained one can evaluate the exact stress field throughout the domain by integration of kernels including the dislocation densities. Therefore, the exact stress intensity at each crack tip can be evaluated.

2.3. Microcrack nucleation criterion

We now take a closer look at the material points around a pre-existing macrocrack. Depending on the type of the material investigated different behaviors can be observed at that region. When polycrystalline materials are considered, one mechanism controlling the response of the crack tip is crack nucleation along grain boundaries. Eventual coalescence of these cracks and crack branching and propagation can also occur. This leads to inevitable crumbling or fracture of the entire material. During this process the load displacement relation may exhibit non-linear behavior. In the present study the relationship between load and/or crack density is examined.

Here we assume the presence of an initial macrocrack and investigate the process of nucleation of microcracks around it. To start the analysis discrete nodal points are considered around the pre-existing macrocrack tip. Each of these points is assigned a random orientation corresponding to the distribution of the grain boundary alignments and a critical stress beyond which a microcrack may nucleate. The distance between the neighboring nodal points and prospective microcrack lengths are much smaller than the pre-existing macrocrack length. The microcrack length and critical stress for each nucleation site can be randomly or uniformly distributed. Initially only crack generation, its effect on the stress intensity factors and displacements, number of generated cracks and applied load relations are considered. Coalescence of microcracks that

develop into a macrocrack, crack propagation and plastic zone development are not included in the model at this stage. After developing a slightly modified model for the kinked interacting cracks these features can be invoked into the analysis.

3. Results and discussions

The numerical analysis carried out consists of a 2D domain containing a pre-existing macrocrack situated at the center of the domain, half of which is depicted in Fig. 1. Possible sites of microcracks are assigned randomly as also shown in Fig. 1. The applied stress is a uniaxial normal stress perpendicular to the main crack line applied far from the crack (at infinity) in most of the cases. The case of a bi-axial state of stress is also considered. The prospective microcrack sizes are taken as 100 times smaller than the main macrocrack length. Having this length smaller or bigger will not affect the generalization of the results because of the non-dimensional form that is explained below. If the half-crack length of the main crack is chosen as the dimensional reference length (or taken as unity) nodal points around the crack tip are taken 0.02 distance away from each other, as shown in Fig. 1. Since the main crack length is treated as finite, the important dimensional parameter for the microcracks is the ratio between the micro and macrocrack lengths. This can be extended to cover the semi-infinite crack case by taking the ratio very small. However direct semi-infinite crack assumption creates a problem of dimension in terms of close tip area. How close one should approach the crack tip (mesh size) to invoke fracture mechanics concepts remains an open question.

The applied stresses are non-dimensionalized by a critical stress σ_c (as can be deduced from Eqs. (8), and (9)) and the unit length scale is considered as the macrocrack length such that $\bar{a}_i = a_i/a_1$, $i \neq 1$ are used in the non-dimensionalization. Actual numbers need to be used for $\bar{a}_i$ during the simulations are mentioned above. This value is chosen to be 0.01 in the present study.

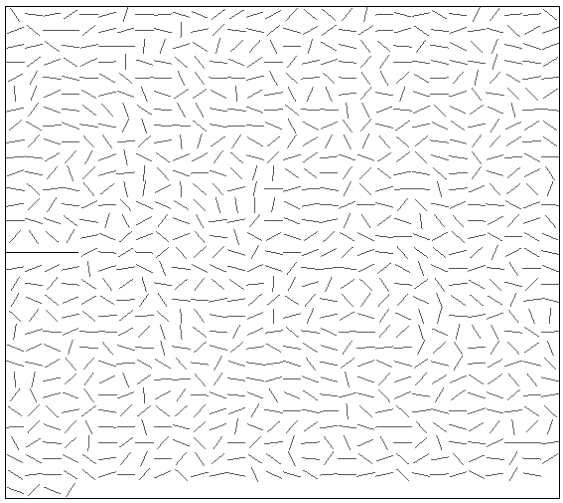

Fig. 1. Representation of the prospective microcrack sites (set 3).

In order to generalize the result for different ranges of macrocrack sizes and applied stresses a load parameter $P = \bar{\sigma}/\sqrt{\bar{a}_i}$ can be defined.

Random distributions of the orientations are assigned. These orientations can be chosen according to a certain statistical distribution, depending on the manufacturing process that results in grains that are aligned along certain directions. Therefore, in addition to completely random distributions, bias orientation distributions, one between $\pm 30°$ and the other between $\pm 20°$ are also investigated. Having these orientations according to a statistical distribution could be done to correlate them with some experimentally observed texture. A similar argument is true for the critical stress that is used to determine crack initiation. The value of the critical stress can also be assumed to be inhomogeneous with a certain distribution form. Different sets of simulations are performed using five different combinations of these distributions. We present the results for 12 cases as follows:

Sets 1 and 3: Two sets of random orientation distributions are considered. Nodes are symmetrically distributed around the upper and lower parts of the main crack line. Total number of nodes checked is 600. The domain is bounded between $x = 0.9$, 1.3 and $y = -1.5$, 1.5.

Set 2: Nodes are non-symmetrically distributed around the macrocrack line. Total number of nodes is 600. The domain is bounded between $x = 0.9$, 1.3 and $y = -2.5$, 0.5.

Sets 4 and 5: Two sets of random orientation distributions are considered. Nodes are symmetrically distributed around the upper and lower parts of the main crack line. Total number of nodes checked is 900. The domain is bounded between $x = 0.9$, 1.5 and $y = -1.5$, 1.5.

Set 6: Random orientations are restricted between $\pm 30°$.

Set 7: Random orientations restricted between $\pm 30°$.

Set 8: Random orientations are restricted between $\pm 20°$.

Set 9: Crack initiation stress (inhomogeneous critical normal stress) changes randomly between 0.5 and 1.5.

Set 10: Orientations are restricted between $\pm 30°$ and crack initiation stress (inhomogeneous critical normal stress) varies randomly between 0.5 and 1.5.

Set S3: Set 3 is repeated by additional crack generation criteria. A critical shear stress value that is the half of the critical normal stress value is added as crack generation criterion. Two more variation of this case is tried with a critical shear stress 0.8 times of the normal and equal to the normal stress. The first two slightly increased the generated crack number and the latter one did not make any significant changes. Therefore only the second one is reported here.

Set 12: All of the above 11 cases are for the uniaxial tension load. Bi-axial loading is considered here by modeling the stress field at the center of a disk under diametrical compression test. The orientation and node distributions are kept the same as in set 3. Two variations of this case are also tried for a critical shear stress similar to case S3.

In all the 1–10 cases microcracks initiate when the normal stress reaches a critical value, which is unity (since the stress is scaled by the critical stress) and the external applied stresses are expressed as fractions of the critical stress. The simulations are performed for a various number of nodes consisting of 400, 600 and 900 nodes. Although higher number of nodes were tried, it was observed that increasing the number of nodes beyond 400 did not change the results.

The nodes are symmetrically distributed around the main crack in four of the cases presented in Fig. 2. Higher number of nodes can be used to make sure that no potential crack site is missed. Choosing the nodes at only above or below the main crack line and using symmetry arguments as

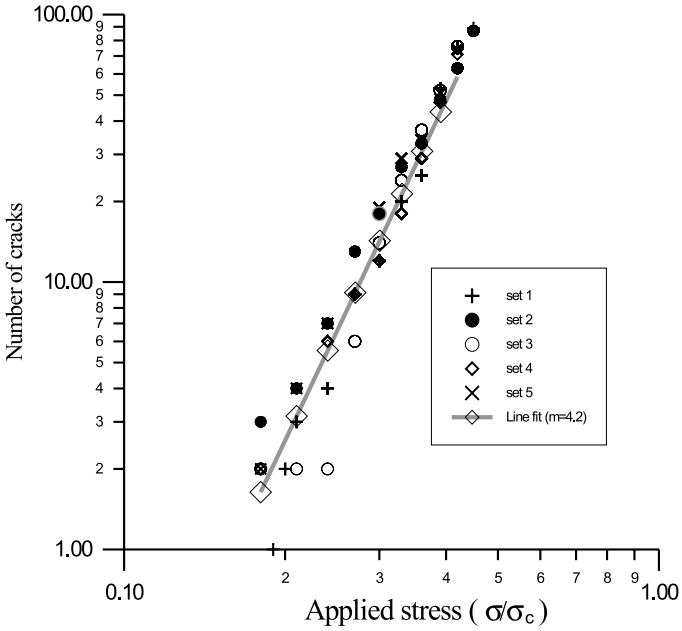

Fig. 2. Plots of applied stress vs. number of microcracks for five different set of random orientations.

done in [1] may reduce the numerical solution effort, however certain boundary conditions along the main crack line must be imposed in that case. The actual case does not necessarily follow that sort of symmetry and the boundary conditions will be unrealistic. Therefore, nodes are considered at both sides of the main crack line.

Fig. 2 shows the applied stress vs. number of microcracks in logarithmic scale. Five different sets of random orientations produce slightly different results. However, the over all results suggest that the relationship between the load and microcrack density is power law of the form:

$$M = C\bar{\sigma}^n, \tag{11}$$

where M is the number of microcracks. Curve fitting gave values for C and the exponent n for sets 1–5 and the result is given in Table 1. The values for n are comparable with the value $n = 4$ reported in [1]. The power "4" arises from the relationship between the "critical" area (the area enclosed by a contour where the principle normal stress is equal to the critical stress) ahead the crack tip and the stress field. Or by simple scaling arguments, since the stress ahead of a crack tip varies as $1/r^{1/2}$ as long as the stress field is not very much affected by perturbation from nearby defects. In the discrete analysis, the stress field is computed explicitly and includes interaction among all cracks and, therefore, it may not vary as $1/r^{1/2}$. Moreover, this scaling argument assumes that the entire area ahead of a *single* crack tip collapses symmetrically in an isotropic and continuum fashion. However, the discrete analysis suggests that microcracking depends on texture and anisotropic properties.

An average least square line fit to all data points given in Fig. 2 produces the following relationship.

Table 1
Model parameters (eq. 11) for various micro-crack distributions

Case	Equation of the line fit
Set 1	$\mathrm{Log}(M) = 5.09\mathrm{Log}(\bar{\sigma}) + 8.69$
Set 2	$\mathrm{Log}(M) = 3.83\mathrm{Log}(\bar{\sigma}) + 7.41$
Set 3	$\mathrm{Log}(M) = 5.11\mathrm{Log}(\bar{\sigma}) + 8.76$
Set 4	$\mathrm{Log}(M) = 4.22\mathrm{Log}(\bar{\sigma}) + 7.72$
Set 5	$\mathrm{Log}(M) = 4.26\mathrm{Log}(\bar{\sigma}) + 7.70$
Set 6	$\mathrm{Log}(M) = 4.62\mathrm{Log}(\bar{\sigma}) + 9.31$
Set 8	$\mathrm{Log}(M) = 4.42\mathrm{Log}(\bar{\sigma}) + 9.17$
Set 9	$\mathrm{Log}(M) = 4.54\mathrm{Log}(\bar{\sigma}) + 8.98$
Set S3	$\mathrm{Log}(M) = 4.85\mathrm{Log}(\bar{\sigma}) + 9.01$

$$M = 2440\bar{\sigma}^{4.12}. \tag{12}$$

It is assumed that potential microcracks have equal lengths. Thus, when the load parameter $P = \bar{\sigma}/\sqrt{\bar{a}_i}$ is used the relation becomes

$$M = 0.172P^{4.12}. \tag{13}$$

It is clear that the equal microcrack length assumption may not always be true as grain sizes and corresponding boundaries could be different as a result the above load parameter P may not be very meaningful.

It is observed that initial stage of microcracking makes a significant difference in the value of the exponent n. If the closer material points to the main crack tip do not have favorable orientations and microcracks initiate closer to the *shielding region*, less number of cracks are expected to nucleate. This in turn affects the earlier stage of microcracking. The simulations are performed up to a certain number of generated microcracks (say up to 200). This gives a satisfactory idea about the response of the cracked medium.

Fig. 3 shows the change in the stress intensity factor (SIF) at the tip of the macrocrack during the microcracking. In Fig. 3, the SIF K_1 at each load level is normalized by K_0, where K_0 is the stress intensity factor corresponding to the macrocrack at that load level but with no microcracks. As can be seen in Fig. 3, five different sets produce different results. In fact in some cases the SIF decreases although the applied stress and the number of cracks are increased. This is due to the shielding and amplification effects of the microcracks. If some microcracks are in the shielding region the SIF at the macrocrack does not increase drastically and even decreases in some cases. Contours defining shielding and amplification regions are discussed in previous studies [3–8]. Furthermore, this figure shows that the distribution and orientations of the microcracks play an important role in the propagation of the main crack. In some cases more microcracks might be more effective in reducing the level of stress intensity at the main crack tip.

Some representative snap shots of the microcracking process at different load levels for set 4 are presented in Fig. 4. The first two microcracks are observed at $\bar{\sigma} = 0.18$ at orientations 13° and 31° at the closest points to the crack tip.

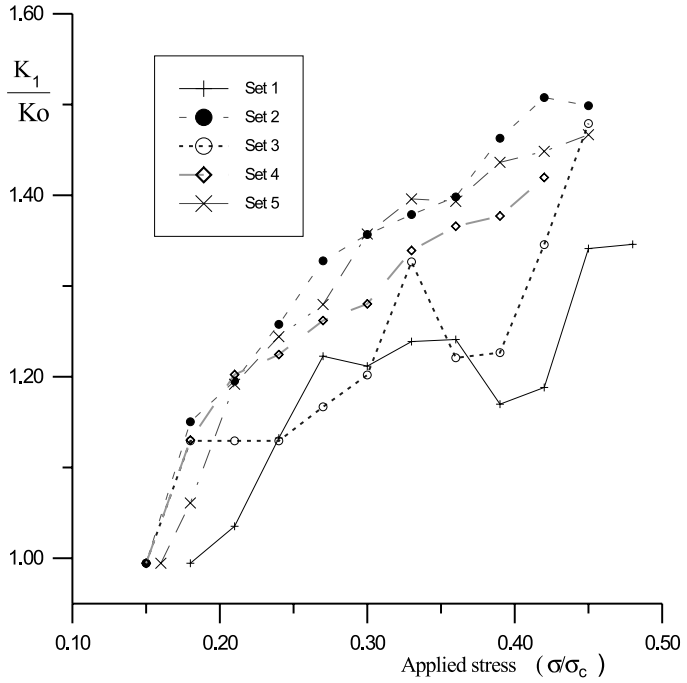

Fig. 3. SIF vs. applied stress plots for five different sets of random orientations (sets 1–5).

The results of sets 6–8 show the effect of biased orientations. As one may expect, biased orientations around 0 (between $\pm 20°$ and $\pm 30°$) resulted into more microcracks when the applied load is normal to the main crack. The resulting microcracking pattern was nearly parallel to the macrocrack. This suggests that the macrocrack would propagate in a nearly self-similar manner with microcracks nucleating parallel to it. As can be seen in Fig. 5(a), sets 6–8 clearly results in more microcracking than the previous five cases.

Next we examine the effect of the critical stress on the result. The critical stress is assumed to be inhomogeneous and randomly distributed around unity (between 0.5 and 1.5) while the orientations are:

(a) completely random (set 9), or

(b) randomly changing between $\pm 30°$ (set 10).

The results are given in Fig. 5(b). Case 9 results in more microcracking than the first five cases. However the number of microcracks is less than the biased orientation cases. This is more significant at especially higher load levels. This can be explained by the fact that when the value of the critical stress is low even at some far *weak* nodes microcracks can nucleate easily, and these sites can trigger more microcracks wherever the critical stress level is low enough. For certain sets of random distribution, e.g. when strong nodes with higher critical stress are mostly concentrated around the macrocrack tip, the behavior could be more similar to the previous cases. Case 10 also resulted in more microcracking because we have more orientations close to being perpendicular to the loading direction.

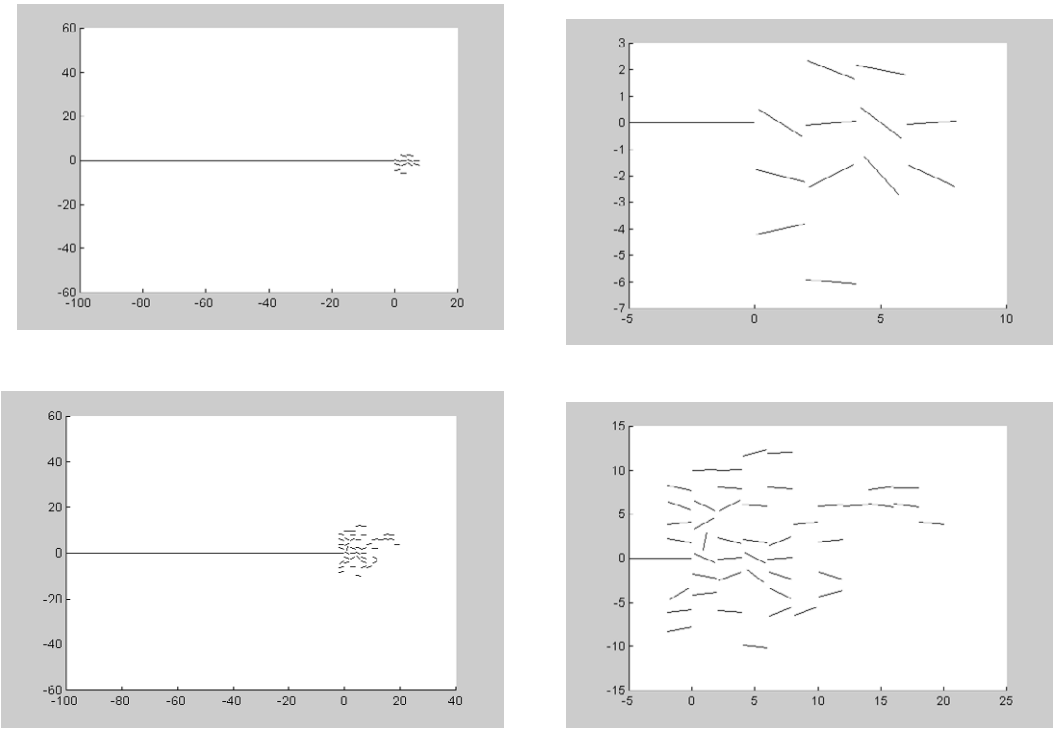

Fig. 4. (a) Microcracks nucleation plots at different steps for set 4. (Applied stress $= 0.3\sigma_c$). Zoomed and scaled plots, (b) Instantaneous plot at applied stress level $= 0.39\sigma_c$ for set 4.

Cracks may initiate because of both normal and shear stresses. The critical normal stress is again taken as unity (or applied stresses are non-dimensionalized by that) and the critical shear stress is

(a) half of the normal stress,
(b) 0.8 times the normal stress, or
(c) the same as the normal stress.

In the cases of (a) and (b) significantly more microcracks are generated even in pure normal (mode I) loading condition. In case (c) slightly more microcracks are generated. This is an expected behavior because there is an additional condition which guarantees that more cracks (equal at least) than the previous criteria will be nucleated. Moreover, along certain orientations shear stresses could be more effective. The applied stress vs. number of microcracks plot for this case is very much similar to the ones in Fig. 5.

In Fig. 6, the effect of the applied stress (or increasing number of microcracks) on the SIF of the main crack tip for some of the later sets is compared with some of the previous cases. It can be deduced from the figure that sets 7 and 8 that result into higher number of microcracks cause more drastic increases in the SIF. The orientations of the microcracks are more responsible for this increase, because microcracks close to being parallel to the main crack are more likely to produce more stress amplification as reported in [8]. As for the case of set S3, more microcracking is observed with increased SIF. However, these effects are not as severe as the biased orientation cases.

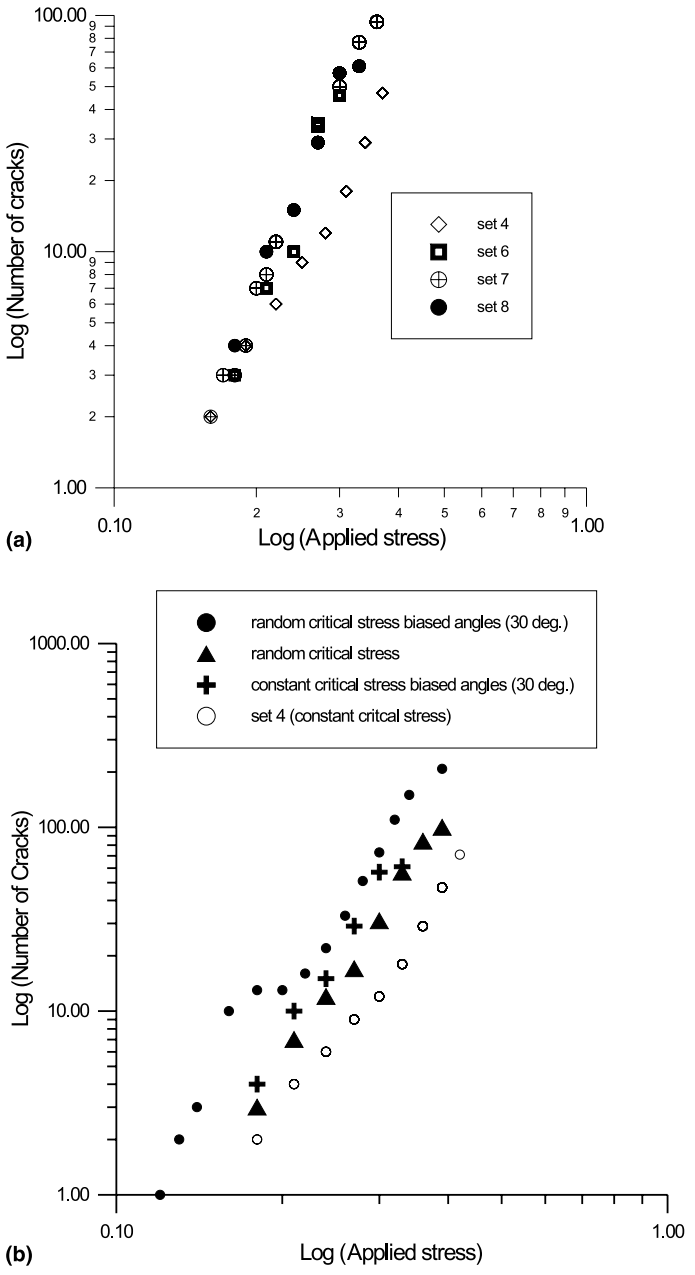

Fig. 5. Comparison of the log plots regular cases, biased orientations, critical stresses and mixed crack generation criterion.

In the numerical simulations, cracks are discretized along their lengths to find dislocation density distributions pointwise (Eqs. (8) and (9)). Although the number of discretization points (N) is important for accuracy, it prolongs the simulation process significantly. In all the simu-

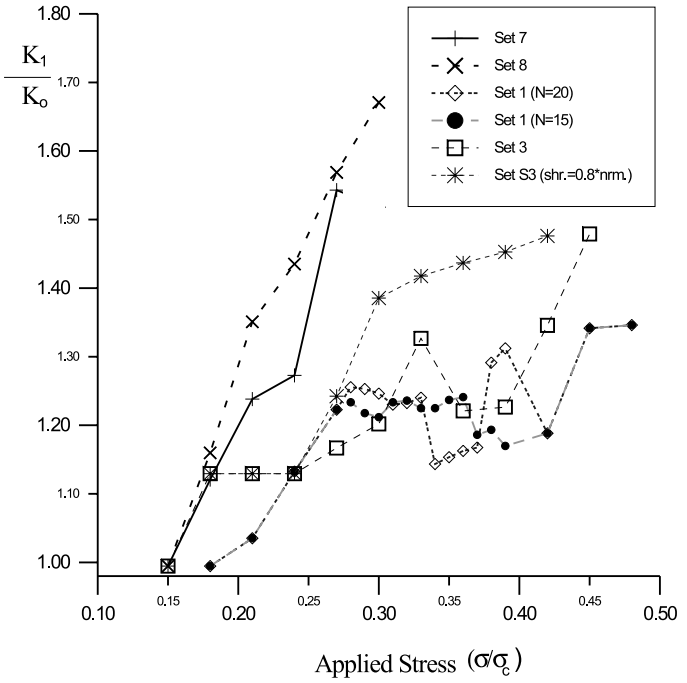

Fig. 6. SIF of the macrocrack vs. applied stress for different cases.

lations discussed so far, we used $N = 15$. In order to see the effect of N on a sample case another run with $N = 20$ is performed for set 1. The effect on the number of generated cracks is not very significant however the effect on the SIF is interesting to observe. As seen in Fig. 6 both cases produce oscillations in the SIF but the path is different. This shows that if the main concern is the accuracy of the SIF rather than the number of cracks, N must be kept high.

It is also possible to follow the history of microcracking and the SIF history at each load level during the numerical process. Since the loading is not performed in a progressive manner, the runs start from a zero microcrack state at each stress level. At a certain fixed load level, an iteration procedure is performed until a steady state is reached. Here a steady state means no more microcracks can nucleate at a constant load. Thus, at the start of the iteration procedure a few microcracks may nucleate, then the stress field is re-evaluated and more new microcracks nucleate, and the process is repeated until no more microcracks can be nucleated. The dashed lines in Fig. 7 indicate the path of the microcracking history. Progressive loading is also analyzed by keeping the same number of microcracks that are generated at each previous load level. Then increasing the load until additional microcracks are nucleated. The number of microcracks turned out to be slightly lower in this latter case, as can be deduced from Fig. 8, but the general trend is the same.

Finally, we examine the effect of bi-axial loading. Bi-axial loading (the stress state at the center of a compressed disk-*Brazilian nut test*) did not make any significant difference when the fracture criterion is based on the normal stress only. However when the shear stress is used together with the normal stress the number of microcracks increased significantly, creating a scattered view of

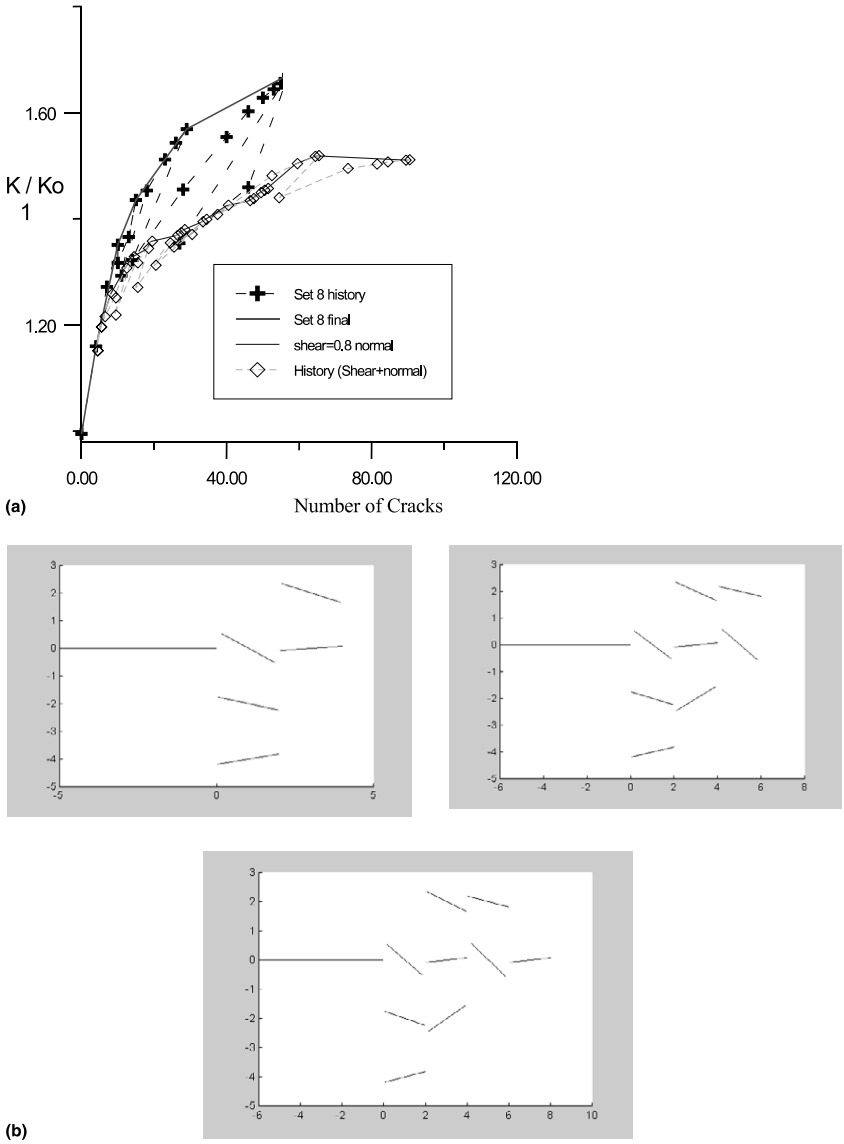

Fig. 7. (a) The effect of microcracking history on SIF of the macrocrack is shown for two sample cases. One case is set 8 the other one is repetition of set 3 for with additional critical shear stress is used in crack generation. (b) Microcracking history samples for set 4 at load level $\sigma_c = 0.27$. The above figure shows first generated cracks. After this the redistribution of the stress field is rechecked and more microcracks nucleate as shown in Figs. 8 and 9(a)–(d).

the generated cracks in terms of both orientations and locations. It is assumed that failure initiates from a pre-existing flaw at the central region where there is a bi-axial state of stress ($3\sigma_{\text{tension}} = \sigma_{\text{comp}}$). Although the stress distribution changes at different positions, it is assumed to be constant over a very small central region. The main crack is aligned perpendicular to the tensile component. The first set of simulations had the same crack ratio. In a second set of runs

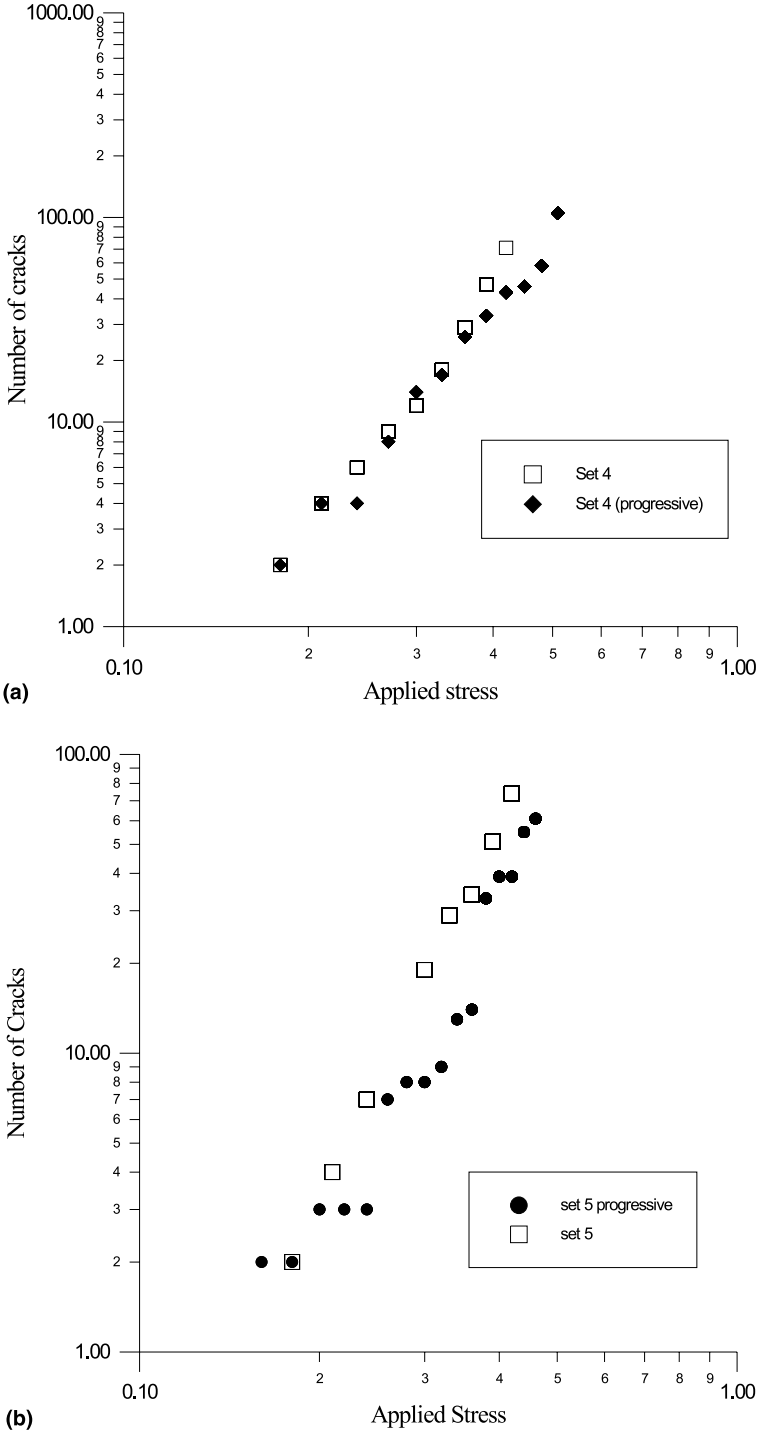

Fig. 8. Effect of loading history on crack density.

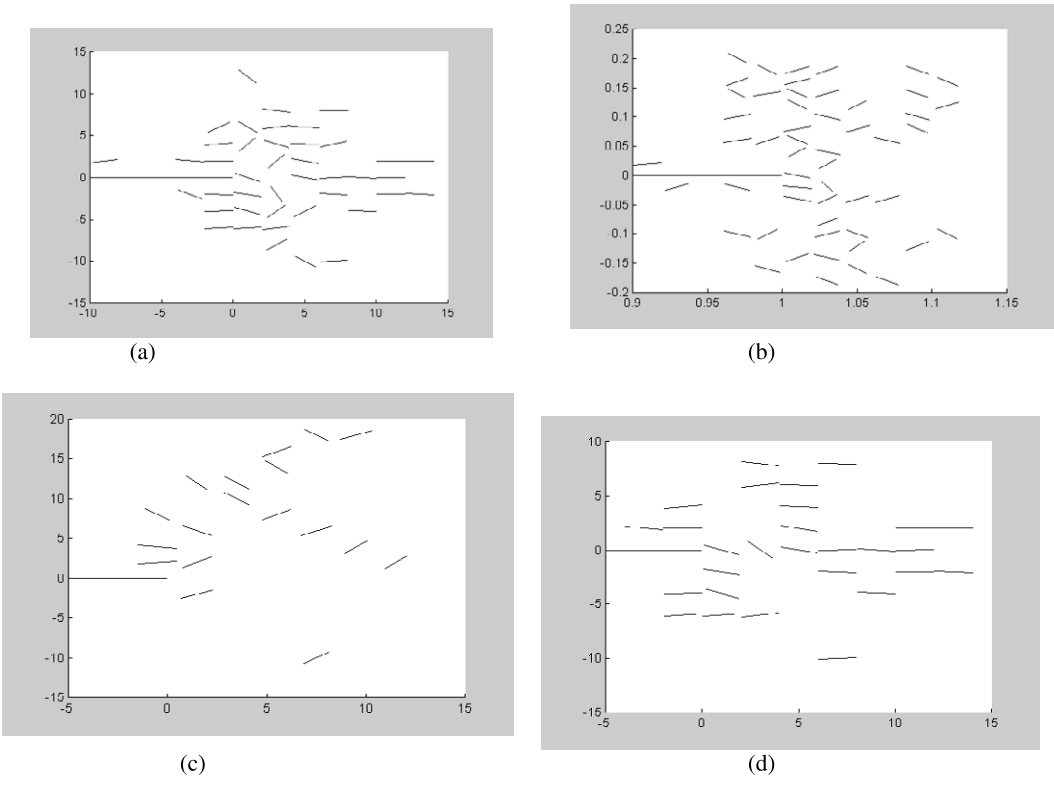

Fig. 9. (a) Microcracks for bi-axial loading case ($\sigma_{comp} = 3\sigma_{tension}$, central field of a disk under diametrical compression) at applied tension stress (opening the main crack) is $\sigma = 0.36\sigma_c$, and the microcrack generation criteria is based on both critical normal and shear that are equal. (b) The same case as in Fig. 8(a). However the critical shear stress for crack initiation is taken as half of the normal one. As seen here the applied tension stress is 0.21 and there are more microcracks. (c) Exactly the same case as 8.a however the shear stress is not used at all. (d) Here the microcrack lengths are 10 times smaller then the main crack in oppose to the 100 times case presented in the other cases. The cracks seen here is created at an applied stress level = 0.47. Both normal and shear critical stresses are used for crack generation criterion. Both of these critical stresses have the same value (unity).

for this specific case the prospective microcrack lengths are taken as 1/10 of the main (initial) crack length. However, when the load parameter P is used the scaling can be unified again. The evolution of microcracks for this case at different load levels is shown in Fig. 8(a). Different cases are tried for the same micro–macrocrack length ratio. When the shear stress is not used in the crack nucleation criteria the number of microcracks is much less than the previously mentioned first five cases. Because the compression stress affects the oblique crack sites negatively, i.e. it works to close the cracks. However, when the effect of the shear stress is also included in the microcracking criterion it is observed that most of the microcracks are generated around 45°, showing the effectiveness of shear in bi-axial loading even if one of the applied stress components is in compression. When the critical shear stress is the same as the normal stress the number of microcracks increases significantly and is close to the first five cases reported. When the value of the critical shear stress is reduced to half of the normal critical stress, even at very low level of

applied stress, many microcracks are generated as can be deduced from Figs. 9(a)–(d). The patterns of generated cracks are also much different when the shear is used as a criterion as can be seen in Figs. 9(a) and (b). The mode II effect is not because of loading only but the interaction is also important in enhancing mode II. Although, in general the normal stresses are considered as more important in brittle materials some critical shear stress could be very important especially in bi-axial loading.

Acknowledgements

The support of the US National Science Foundation under grant number CMS-9634726 to Zbib, and the partial support of the Pacific Northwest National Laboratory to Demir during the summer of 1998 is gratefully acknowledged.

Appendix A

The kernels that appears in Eqs. (8) and (9) and related geometric parameters are given as follows:

$$N_{ij}^{n} = \frac{\cos\theta_{ij}}{r_{ij}} - \frac{\sin\theta_{ij}}{r_{ij}}\sin(2\gamma_{ij}),$$

$$T_{ij}^{n} = -\frac{\sin\theta_{ij}}{r_{ij}} - \frac{\cos\theta_{ij}}{r_{ij}}\sin(2\gamma_{ij}),$$

$$N_{ij}^{t} = \frac{\sin\theta_{ij}}{r_{ij}}\cos(2\gamma_{ij}),$$

$$T_{ij}^{t} = \frac{\cos\theta_{ij}}{r_{ij}}\cos(2\gamma_{ij}),$$

$$x_{ci} = \bar{x}_i\cos\alpha_i + \bar{y}_i\sin\alpha_i, \quad y_{ci} = \bar{y}_i\cos\alpha_i - \bar{x}_i\sin\alpha_i,$$

where $\bar{x}_i$ and $\bar{y}_i$ are the position of the center and α_i is the orientation of crack i measured in the global coordinate system.

$$x_{c_{ij}} = x_{cj} - x_{ci}, \quad y_{c_{ij}} = y_{cj} - y_{ci},$$

$$c_{ij}^2 = x_{c_{ij}}^2 + y_{c_{ij}}^2,$$

$$\theta_{c_{ij}} = \tan^{-1}\left(\frac{y_{c_{ij}}}{x_{c_{ij}}}\right),$$

$$x_{ij} = x_i - (s_i \cos(\alpha_{ij}) + x_{c_{ij}}),$$

$$y_{ij} = -(s_i \sin(\alpha_{ij}) + y_{c_{ij}}),$$

$$r_{ij} = \sqrt{x_{ij}^2 + y_{ij}^2}, \quad \cos\theta'_{ij} = \frac{x_{ij}}{r_{ij}}, \quad \sin\theta'_{ij} = \frac{y_{ij}}{r_{ij}},$$

$$\theta_{ij} = \theta'_{ij} - \alpha_{ij}, \quad \gamma_{ij} = -\theta'_{ij},$$

where s_j is the point where a dislocation with the strength $b(s)\,\mathrm{d}s$ that is taken out of continuous dislocation distribution along crack j is located and x_i is the point where the stresses due to this piece of dislocation density is written. All the other parameters are shown in Fig. 10 on any two cracks i and j located on the planar domain ahead of the main crack. Point x_i can be any point on the domain in general. However Fig. 10 and Appendix A is used specifically to write the integral equations where the basic interest is to express the stresses along the line of crack i. Therefore in Fig. 10 x_i is shown on that crack line.

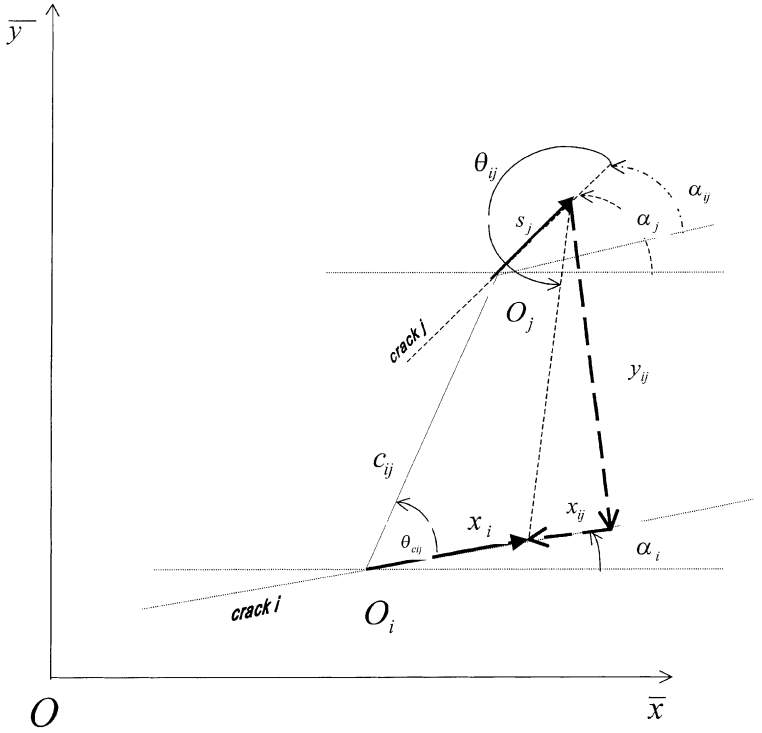

Fig. 10. The representation of the geometric parameters used in the kernels of the integral equations.

References

[1] R.G. Hoagland, J.D. Embury, A treatment of inelastic deformation around a crack tip due to microcracking, J. Am. Ceram. Soc. 63 (7–8) (1980) 404–410.
[2] R.G. Hoagland, J.D. Embury, On the density of microcracks formed during the fracture of ceramics, Scripta Met. 9 (1975) 907–909.
[3] S.X. Gong, H. Horii, General solution to the problem of microcracks near the tip of a main crack, J. Mech. Phys. Solids 37 (1975) 27–46.
[4] K.Y. Lam, C. Wen, Z. Tao, Interaction between microcracks and a main crack in a semi-infinite medium, Eng. Frac. Mech. 44 (5) (1993) 753–761.
[5] L.R.F. Rose, Microcrack interaction with a main crack, Int. J. Fract 31 (1986) 233–242.
[6] R.R. Rubinstein, Macrocrack–microdefect interaction, J. Appl. Mech. 53 (1986) 505–510.
[7] C. Wen, K.Y. Lam, Effect of multiflat inclusions on stress intensity factor of a semi-infinite crack, Eng. Frac. Mech. 47 (2) (1986) 157–168.
[8] I. Demir, Interaction between finite planar cracks, King Saud University Journal, vol. 11. Eng. Sci. (1) (1998) 85–116.
[9] H.M. Zbib, I. Demir, The interface ring dislocation in fiber–matrix composites: approximate analytical solution, ASME J. Eng. Mater. Technol. 116 (1994) 279–285.
[10] S. Close, H.M. Zbib, The stress intensity factors and interactions between cylindrical cracks in fiber–matrix composites an invited article, in: G.Z. Voyiadjis, D.H. Allen (Eds.), in: Damage and Interfacial Debonding in Composites, Elsevier Science, The Netherlands, 1996, pp. 3–27.
[11] I. Demir, A.N. Gulluoglu, Dislocation dynamics simulations in the presence of interacting cracks, ASME J. Mater. Sci. Technol. 121 (1999) 151–155.
[12] H.M. Zbib, M. Rhee, J.P. Hirth, On plastic deformation and the dynamcis of 3D dislocations, Int. J. Mech. Sci. 40 (1998) 113–127.
[13] J.P. Hirth, J. Lothe, Theory of Dislocations, Wiley, New York, 1982.
[14] F. Erdogan, G. Gupta, On the numerical solution of singular integral equations, Quart. Appl. Math. 30 (1972) 525–535.